Talanta 254 (2023) 124134

Contents lists available at ScienceDirect

Talanta

journal homepage: www.elsevier.com/locate/talanta

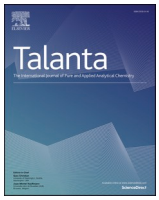

PB@PDA nanocomposites as nanolabels and signal reporters for separate-type cathodic photoelectrochemical immunosensors in the detection of carcinoembryonic antigens

Xiaodi Zhu [a,1], Jingkai Shan [a,1], Li Dai [a], Feifei Shi [a], Jinshen Wang [b], Huan Wang [a], Yuyang Li [a], Dan Wu [a], Hongmin Ma [a,*], Qin Wei [a,**], Huangxian Ju [a,c]

[a] Collaborative Innovation Center for Green Chemical Manufacturing and Accurate Detection; Key Laboratory of Interfacial Reaction & Sensing Analysis in Universities of Shandong, School of Chemistry and Chemical Engineering, University of Jinan, Jinan, 250022, Shandong. China
[b] Department of Rehabilitation, Shandong Provincial Hospital Affiliated to Shandong First Medical University, Jinan, 250021, Shandong, China
[c] State Key Laboratory of Analytical Chemistry for Life Science, Department of Chemistry, Nanjing University, Nanjing, 210023, PR China

ARTICLE INFO

Keywords:
Prussian blue
Polydopamine
ELISA
Photoelectrochemical biosensor
Tumor marker

ABSTRACT

Photoelectrochemical (PEC) immunoassays exhibiting high sensitivity and decent operability have considerable potential in areas such as cancer diagnostics. In particular, cathodic PEC configurations can prevent interference from reductive substances, which can occur in biological samples; however, challenges remain in terms of sensitivity and operability. In this study, separate-type PEC immunoassays were developed for carcinoembryonic antigen (CEA) by combining microplate-based immune recognition and off–on cathodic PEC detection. Polydopamine (PDA)-coated Prussian blue (PB) nanoparticles (PB@PDA NPs) were used as signal tags to label the detection antibody. The PB NPs and PDA captured on the microplates both disassembled under strongly alkaline conditions to generate redox-active electron acceptors. The disassembled products were quantitatively transferred to PEC detection cells and synergistically enhanced the PEC current with microstructured BiOI, which operated as a cathodic semiconductor electrode. As proof of principle, carcinoembryonic antigen (CEA) was applied to elucidate the potential application of PEC immunoassay in clinical diagnosis, and the obtained linear range of the sensor was 0.001–100 ng mL^{-1} with the detection limit of 54.9 fg mL^{-1} (S/N = 3). The proposed separate-type off–on PEC strategy showed high sensitivity and decent operability for CEA detection, indicating its potential for the identification of other tumor markers.

1. Introduction

Immunoassays with sandwich-type configurations have been remarkably successful in the *in vitro* detection of protein tumor markers owing to the effective biorecognition of analytical targets by complex matrices [1,2]. The well-established enzyme-linked immunosorbent assay (ELISA) uses microplates as detection platforms and enzymes as catalytic labels. Moreover, the integration of microplate readers with automated incubation and sampling processes has enabled high-throughput analysis [3,4]. However, significant challenges remain in terms of achieving high detection sensitivities and wide response ranges of color-based output signals. Consequently, immune-recognition configurations have been combined with other optical and electrochemical techniques to construct high-sensitivity sensing platforms, such as electrochemical (EC) [5,6], electrochemiluminescent (ECL) [7–9], and photoelectrochemical (PEC) [10–12] immunosensors. Additionally, nanomaterials show tremendous promise as signal tags (i.e., nanolabels) in these methods because of their unique and diverse physicochemical properties.

PEC immunoassays have attracted considerable attention because of their minimal interference from input signals and inherently high sensitivity for electrochemical detection [13]. Both anodic and cathodic PEC immunosensors have been developed using different semiconductor materials as photoelectrochemically active transducers [14,15]. In the

* Corresponding author.
** Corresponding author.
E-mail addresses: chm_mahm@ujn.edu.cn (H. Ma), sdjndxwq@163.com (Q. Wei).
[1] Xiaodi Zhu and Jingkai Shan contributed equally to this work.

https://doi.org/10.1016/j.talanta.2022.124134
Received 4 November 2022; Received in revised form 21 November 2022; Accepted 22 November 2022
Available online 23 November 2022

anodic PEC detection mode, electron donors in the electrolyte are essential for generating a stable anodic PEC current. In contrast, cathodic PEC detection is based on the removal of photogenerated electrons. The dissolved oxygen in the solution acts as an electron acceptor in cathodic PEC detection. However, PEC efficiency is low, and reproducibility cannot be guaranteed [16]. Certain redox-active substances are known to act as electron acceptors for PEC biosensors [16,17]. Generally, the on–off detection mode is adopted in scenarios with decreasing current signals. However, despite the advantages related to their high detection sensitivities, cathodic PEC immunosensors operating in the off–on detection mode have been scarcely reported because of the difficulties involved in using electron acceptors as signal tags. Additionally, the complicated construction of PEC electrodes, which is currently incompatible with automated devices, is an issue. Therefore, microplate-based immune recognition was combined with cathodic PEC detection in this study to develop separate-type immunoassays (Scheme 1) with redox-active nanocomposites as nanolabels and electron acceptors.

Prussian blue (PB) has been extensively used in electrochemical [18–20] and optical bioassays [21–23] owing to its excellent redox and catalytic properties. Additionally, the size and morphology of PB nanoparticles can be controlled to facilitate their use as nanolabels for immunoassays. However, difficulties related to their bioconjugation with biomolecules hinder their applications. Strategies such as the use of mussel-inspired polydopamine (PDA) coatings, which have been developed as a universal surface modification approach for solids and nanomaterials, can be adopted to address this issue [24]. PDA-based surface engineering of a PEC sensing platform was demonstrated in our previous study, along with its feasibility and convenience for immobilization of biorecognition elements [25–27]. In the present study, PDA-coated PB nanoparticles (PB@PDA NPs) were used as signal tags for immunoassays. PB@PDA can be employed as a theranostic agent for both cancer imaging [28,29] and photothermal therapy [30–32]. However, the use of PB@PDA as a source of electron acceptors in cathodic PEC bioassays has been scarcely reported.

Carcinoembryonic antigen (CEA) is an important biomarker that can be used for diagnosing gastric cancer, colorectal cancer, breast cancer and other gynecological tumors [33,34]. Furthermore, the CEA level is an index to evaluate the success of operation and the prognosis of patients. Therefore, to validate the feasibility of the proposed detection strategy, a broad-spectrum tumor marker—CEA [35]—was used as a model analytical target for the immunoassay. Unexpectedly, both PDA and PB enhanced the cathodic PEC response, leading to a decent analytical performance. Overall, the separate-type immunoassays enabled off–on cathodic PEC detection with high sensitivity and adequate reproducibility. Moreover, the combination of a redox-active polymer with redox-active nanoparticles not only facilitated the bioconjugation of PB as a nanolabel, but also synergistically enhanced the PEC response. Additionally, the consistent disassembly-related properties of PDA and PB under alkaline conditions were exploited to produce different types of electron acceptors.

2. Material and methods

2.1. Materials and chemicals

Bismuth nitrate pentahydrate, Potassium iodide, Polyvinylpyrrolidone (PVP, K30), Dopamine hydrochloride, Sodium hydroxide, Tris (hydroxymethyl)aminomethane (Tris), Disodium hydrogen phosphate and Potassium dihydrogen phosphate were purchased from Shanghai Macklin Biochemical Chemical Reagent Co., Ltd. Potassium ferricyanide was purchased from Sinopharm Chemical Reagent Beijing Co., Ltd, China. Ethylene glycol (EG) and ethanol were purchased from Tianjin Fuyu Fine Chemical Co., Ltd. Bovine serum albumin was provided by Shanghai Aladdin Biochemical Reagent Co., Ltd. Carcinoembryonic antigen (CEA) antigen and antibody were purchased from Shanghai Linc-Bio Science Co. LTD. The working electrode adopts indium tin oxide (ITO) glass provided by China Southern Glass Group Co., Ltd. All reagents in this work are of analytical grade.

2.2. Synthesis of Bismuth oxyiodide (BiOI) microspheres

BiOI was synthesized using a previously reported protocol [36] with slight modifications. First, $Bi(NO_3)_3$ $5H_2O$ was added to EG (40 mL) and

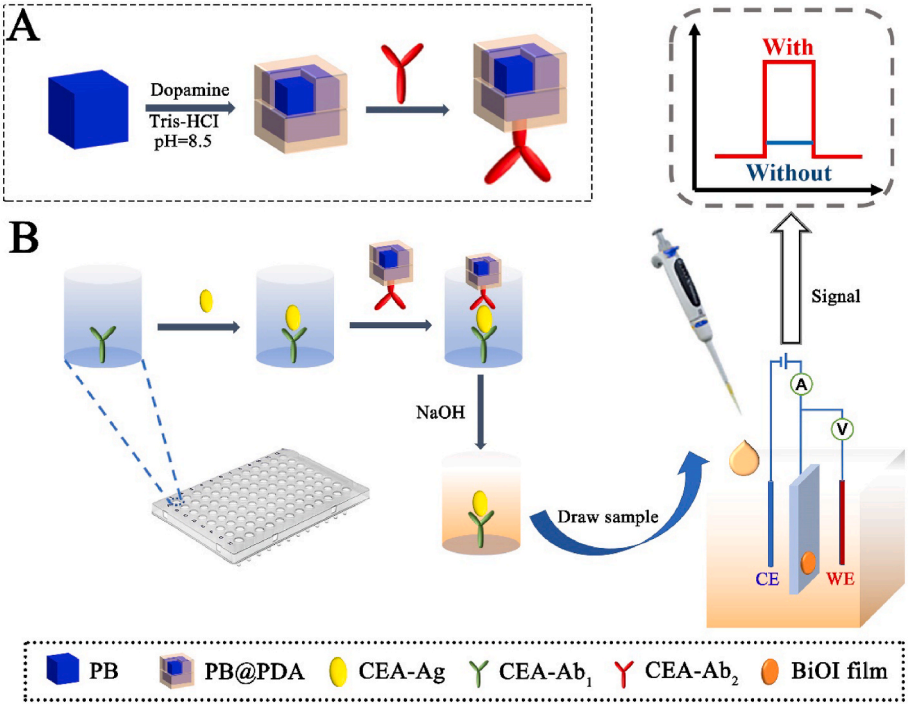

Scheme 1. (A) Preparation of secondary antibody marker PB@PDA–Ab_2 and (B) construction of the PEC sensor.

stirred to ensure dissolution, resulting in solution A (0.1 M). Next, KI was added to EG (40 mL) and stirred in the dark to ensure dissolution, yielding solution B (0.1 M). Solution B was added to solution A, stirred for 30 min in the dark, transferred to a 100 mL reaction kettle, and heated at 160 °C for 12 h. After cooling to room temperature, a yellow precipitate was collected by centrifugation and subsequently washed three times with ethanol and deionized water to remove unreacted material. Finally, the precipitate was dried in a vacuum oven at 80 °C for 12 h and stored at 4 °C for subsequent use.

2.3. Preparation of PB NPs

PB NPs were synthesized according to the literature [37] with slight modifications. First, PVP (8.0 g) was added to a HCl solution (1 M, 40 mL) and stirred to ensure dissolution. Next, potassium ferricyanide (0.696 g) was dissolved in the preceding solution, and the mixed solution was transferred to a 50 mL reaction kettle and heated at 100 °C for 24 h. After cooling to room temperature, a blue precipitate was collected by centrifugation and washed three times with ethanol and ultrapure water to remove unreacted substances, such as PVP. Finally, the PB NPs were dried in a vacuum oven for 12 h to remove moisture and stored at 4 °C for subsequent use.

2.4. Preparation of PB@PDA NPs

PB@PDA NPs were prepared by exploiting the tendency of dopamine to form a stable and uniform polydopamine film on NP surfaces under alkaline aerobic conditions. Five milligrams each of the PB NPs and dopamine hydrochloride were added to a Tris-HCl buffer solution (5 mL; pH = 8.5; 0.01 M) and reacted under aerobic conditions for 2 h. The resulting solution was centrifuged, and the product was washed three times with deionized water, dispersed in a phosphate-buffered saline (PBS) solution (4 mL; pH = 7.4; 0.1 M), and stored at 4 °C for subsequent use.

2.5. Preparation of preparation of PB@PDA-Ab_2

The preparation of PB@PDA-Ab_2 is illustrated in Scheme 1A. The detection antibody (Ab_2; 1 μg mL^{-1}, 1 mL) was added to the PB@PDA NP dispersion (4 mL) and incubated at 4 °C under agitation for 12 h. A blue precipitate was collected by centrifugation and washed three times with a PBS solution (pH 7.4, 0.1 M). Subsequently, the product was added to a bovine serum albumin (BSA) solution (5 mL, 1% in PBS solvent), centrifuged, and washed three times with PBS. Finally, the precipitate was dispersed in PBS (5 mL) at 4 °C for subsequent use.

2.6. Characterization

The PB NP and PB@PDA NP samples (1 mg mL^{-1}) were diluted tenfold with deionized water, and their diameters were estimated by dynamic light scattering (DLS; Nano ZS particle size analyzer; Malvern, UK).

For field-emission scanning electron microscopy (SEM; Zeiss, Germany), sample analysis was conducted by fixing BiOI powder to the spike-shaped sample stage of the SEM device using conductive glue.

For transmission electron microscopy (TEM; JEM-2100; JEOL, Japan), a drop of the NP dispersion (8 μL) was added to a copper grid coated with a continuous layer of carbon using a pipette, and the dried copper mesh was subsequently imaged.

X-ray diffraction (XRD) patterns of the BiOI and PB powders were obtained using a Bruker device (Germany).

Absorption spectra were obtained using a TU-1901 UV–vis spectrophotometer (Puxi Instrument, Beijing).

2.7. Preparation of PEC biosensor

The construction of the identification platform of the PEC sensor is described henceforth (Scheme 1B). First, a capture antibody (Ab_1; 100 μL) was added to a 96-well plate, incubated at 4 °C for 12 h, and washed three times with PBS (0.1 M, pH 7.4). A BSA solution (1%, 100 μL) was subsequently added, and the system was incubated at 37 °C for 1 h and washed three times with PBS. Then, the CEA antigen was added at different concentrations in a manner similar to that for the BSA solution. Finally, the PB@PDA–Ab_2 dispersion was added, and the previous experimental step was repeated.

To construct the detection platform of the PEC sensor, a BiOI dispersion (4 mg mL^{-1}) was first prepared by dissolving the BiOI microspheres (4 mg) in deionized water (1 mL). The BiOI dispersion droplets (10 μL) were placed on a treated indium-tin-oxide (ITO) working electrode and dried, yielding a BiOI photocathode electrode. A NaOH solution (100 μL, 0.1 M) was added to the treated 96-well plate to decompose the PB@PDA NPs on the microplate using ELISA to generate ferricyanide. The decomposed solution in the microplate was subsequently added to a Tris-HCl buffer solution (4900 μL, pH = 6.5, 0.01 M), and the resulting solution was subjected to photoelectrochemical detection using the BiOI photocathode.

2.8. Preparation of the real samples

For real sample analysis, blood (from Shandong Provincial Hospital Affiliated to Shandong First Medical University) was run at 3000 r/min for 10 min. The serum from the upper layer was diluted twice for spiking experiments. Sample A was taken from patients with gastric cancer, and sample B was taken from patients with rectal cancer after surgical treatment. First, the content of CEA in serum was determined. Then, the serum samples were added with different concentrations of standard CEA for determination.

2.9. Photocurrent detection

A traditional three-electrode system consisting of a saturated calomel electrode, platinum wire, and the constructed PEC biosensor as the reference, counter, and working electrodes, respectively, was used for detection, with a Tris-HCl buffer solution (0.01 M, pH 6.5) as the electrolyte. The PEC tests were performed at 25 °C using a Zahner photoelectrochemical test system (Zennium-PP 211, Germany) with the bias voltage set to 0 V, a full-wavelength light source, and excitation light power of 1000 W m^{-2}.

3. Results and discussion

3.1. Characterization of BiOI microspheres

BiOI has a typical layered structure with superimposed $[Bi_2O_2]^{2+}$ layers and iodide ions and a conventional 2D nanosheet morphology. However, an appropriate solvent can induce self-assembly of the nanosheets, transforming BiOI from 2D layered nanosheets to 3D mesoporous microflowers, which significantly increases the specific surface area [16]. BiOI was synthesized using a hydrothermal method with EG as the solvent. SEM analysis (Fig. 1A) indicated that the prepared BiOI was in the form of ~1-μm-sized flower-like microspheres comprising closely arranged sheet-like 2D structures. Moreover, XRD peaks of BiOI were observed at 29.7°, 31.7°, 45.5°, 51.5°, and 55.3° (Fig. 2B), which corresponded to the standard card of tetragonal BiOI [JCPDS No. 70–2062; (012), (110), (013), (112), (020) (014) (021), and (122), respectively]. These results confirmed the successful preparation of flower-like BiOI microspheres.

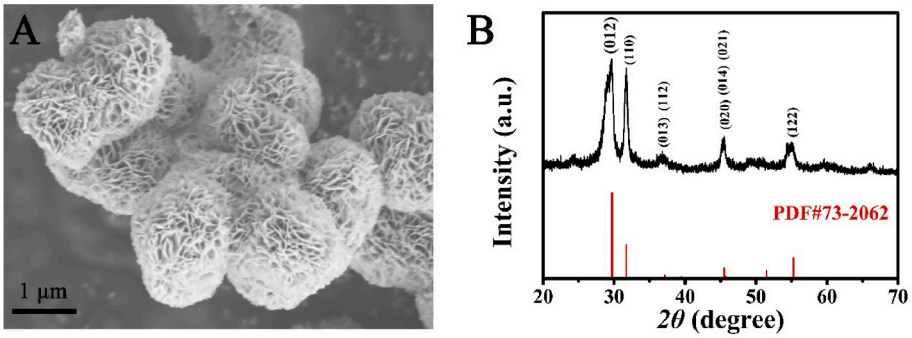

Fig. 1. (A) SEM image and (B) XRD pattern of flower-shaped BiOI microspheres.

3.2. Characterization of PB and PB@PDA NPs

Cubic PB NPs were synthesized under acidic conditions using PVP as the stabilizer and reducing agent, and potassium ferricyanide as the sole iron source. The morphologies of the PB and PB@PDA NPs were examined by TEM and DLS, which revealed ~200-nm-sized cubes of PB [Fig. 2A, B]. In biosensing, the negatively charged PB NP surface can directly bind to antibodies; however, the complex spatial structures of the antibodies of certain biological macromolecules can hinder this binding. Therefore, a PDA film was introduced to facilitate the binding between the PB NPs and antibodies. PDAs inspired by mussel adhesion proteins can adhere to most substrate surfaces and form homogeneous films [24]. Additionally, PDA can undergo Michael addition and/or Schiff base reactions with amine-containing molecules, enabling strong binding with antibodies through chemical bonds. TEM analysis of the PB@PDA NPs [Fig. 2C, D] suggested that the PB NP surface was enveloped by a thin film, that is, PDA. DLS spectra of the pristine and PDA-coated PB NPs reflected the changes in diameter of the NPs [Fig. 2E, F]. Moreover, changes in the UV–vis region in the UV–vis absorption spectra (Fig. 2H) further corroborated the coating of the PDA film on the PB NP surface. Powder XRD analysis (Fig. 2G) revealed the crystal structure of the PB NPs. The diffraction peaks of the PB NPs at 17.5°, 24.8°, 35.5°, 39.8°, 43.7°, 50.9°, 54.3°, and 57.5° corresponded to the (200), (220), (400), (420), (422), (440), (600), and (620) crystal planes in the standard card of PB (JCPDS No.73-0687).

3.3. Photochemical tests and signal generation mechanism of BiOI/ITO electrode

As a narrow-bandgap p-type semiconductor, BiOI has attracted extensive attention owing to its strong absorption in the visible-light region and decent chemical stability. In this study, the $[Fe(CN)_6]^{3-}$/$[Fe(CN)_6]^{4-}$ electron pair was used instead of O_2/O_2^- to improve the photocurrent response of the BiOI electrode. The addition of potassium ferricyanide significantly improved the photocurrent response of the BiOI electrode (Fig. 3A), and the photocurrent signal generated by the PB NPs after NaOH addition was significantly higher than that of the pristine PB NPs (Fig. 3B). This indicates that the $[Fe(CN)_6]^{3-}$ generated via the decomposition of the PB NPs enhanced the photocurrent response of the BiOI electrodes. Additionally, the photocurrent signal of the BiOI electrode increased further after the PDA coating, because the PDA film is a redox composite film and the quinoid structure in the dissociated PDA molecule can be reduced to an electron-containing phenolic structure. Therefore, as shown in the electron-transfer mechanism (Fig. 3C), both $[Fe(CN)_6]^{3-}$ and PDA acted as electron acceptors to capture electrons, enhancing the photocurrent response of BiOI [38]. The differences in the photocurrent signals of the BiOI electrode in different electrolytes (Fig. 3B) indicate that the ferricyanide generated via the decomposition of the PB@PDA NPs under alkaline conditions and the PDA redox composite film exhibited a synergistic enhancement effect, which significantly improved the photocurrent signal of the BiOI electrode. UV–vis absorption spectroscopy was performed to explore the possible effects of the PDA film coating on the decomposition of the PB NPs (Fig. 3D). Upon the addition of NaOH, the characteristic peak of PB@PDA NPs at 750 nm disappeared, indicating that the addition of PDA did not affect the decomposition of the PB NPs, which was also corroborated by a color change (inset of Fig. 3D).

3.4. Selection of conditions for the PEC biosensor

The pH of NaOH, which was used as an alkali source to decompose the PB NPs, was varied to determine an optimal value for complete decomposition of the PB NPs. The pH was found to considerably influence the generation and amplification of the signal. The absorption peak of PB at 750 nm gradually decreased with increasing pH of NaOH, with the peak disappearing completely at a pH of 13. Therefore, an NaOH solution with a pH of 13 was used for the decomposition. The thickness of the PDA film is another important factor that affects the generation of electron donors via PB NP decomposition. The NaOH solution was added to the PB@PDA NP dispersions corresponding to different PDA-film-coating durations to investigate the decomposition, along with a Tris-HCl buffer solution, and the mixed solution was used as the electrolyte. The BiOI electrode exhibited an optimal signal in the electrolyte corresponding to a PDA wrapping duration of 2 h; therefore, a reaction time of 2 h was adopted. The acidity and alkalinity of electrolytes significantly influence the signal generated by an electrode. Therefore, the pH of the Tris-HCl buffer added during the PEC tests was varied (Fig. 4C), which revealed that the solution with a pH of 6.5 exhibited an optimal signal. UV–vis absorption tests of the electrolytes (Fig. 4D) corresponding to Fig. 4C data suggested that the change in pH of the Tris-HCl buffer did not affect the stability of the electrolyte solution but influenced the photocurrent response of the BiOI electrode.

3.5. Response of PEC sensor to CEA

Under the optimized experimental conditions, different CEA concentrations were detected using the PEC sensor. As the CEA concentration increased, a greater number of PB@PDA NPs were bound in the 96-well plate and the photocurrent signal gradually increased (Fig. 5). The logarithm of CEA concentration in the range of 0.001–100 ng mL^{-1} was linearly related to the photocurrent of the BiOI electrode. The detection range of the PEC sensor for CEA was 0.001–100 ng mL^{-1} and the detection limit was 54.9 fg mL^{-1} (S/N = 3). The regression equation of the calibration curve was $I_1 = -0.252 \cdot \lg c - 1.96$, and the correlation coefficient was 0.996.

3.6. Stability and anti-interference tests of the PEC biosensor

The stability of the photocurrent response of the prepared immunosensor was subsequently investigated (Fig. 6A). At a CEA

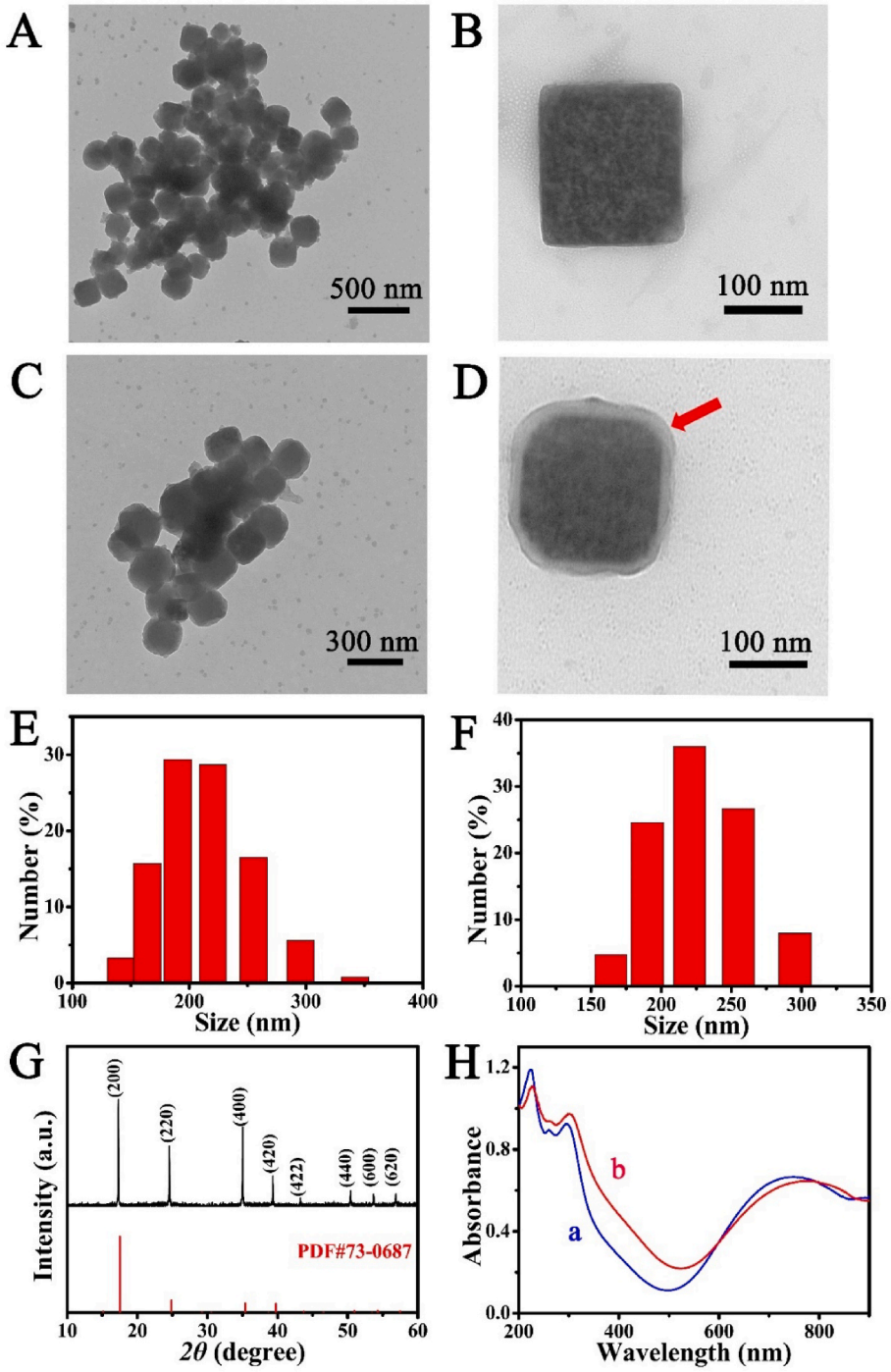

Fig. 2. TEM images of the (A, B) PB and (C, D) PB@PDA NPs; DLS spectra of the (E) PB and (F) PB@PDA NPs; (G) XRD pattern of the PB NPs; (H) UV–vis absorption spectra of the (a) PB and (b) PB@PDA NPs.

concentration of 0.1 ng mL^{-1}, the photocurrent response was investigated for 15 cycles with an on–off irradiation time of 300 s. The signals corresponding to the pure interfering proteins were equivalent to the blank signal [Fig. 6B(c–e)]. Moreover, the signals corresponding to the CEA-added specimens did not change significantly compared to that of pure CEA, indicating that the constructed sensor exhibited decent selectivity and specificity for CEA. Additionally, the detection limit of the CEA assay was superior to those previously reported (Table 1), highlighting the high sensitivity of the constructed sensor.

3.7. Real-sample analysis

To analyze the applicability of the constructed PEC biosensor in practical analysis, the recoveries of different concentrations of CEA in different serum samples were tested. As shown in Table 2, the recovery of different concentrations of CEA in sample A ranged from 95.0 to 100.0%, and the RSD range was from 1.5 to 2.3; the recovery of different concentrations of CEA in sample B ranged from 100.0 to 105.0%, and the RSD range was from 1.1 to 1.3. The above data showed that the sensor had good accuracy and practicability.

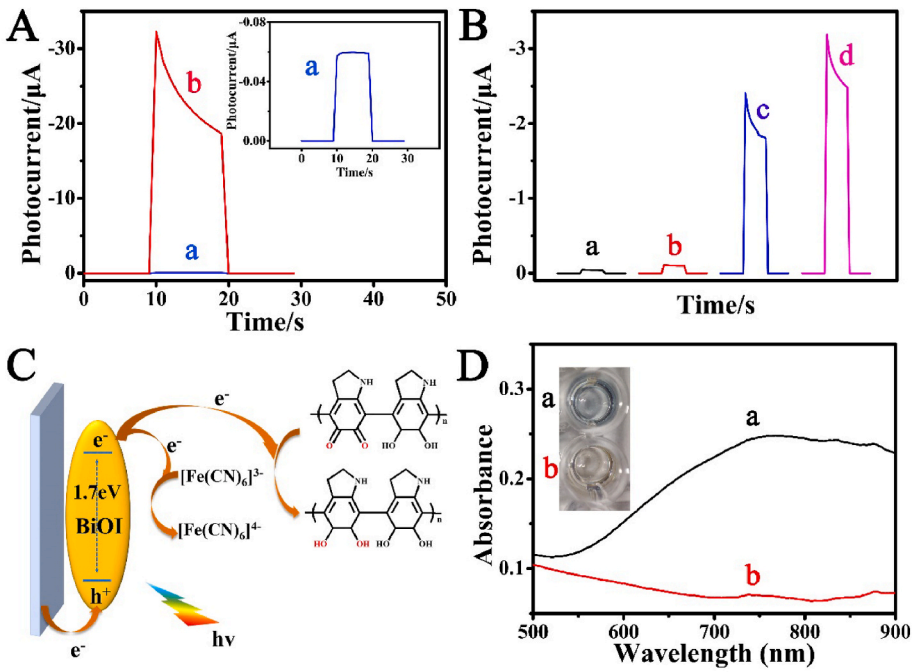

Fig. 3. (A) Photocurrent response of BiOI/ITO electrode in a Tris-HCl solution (a) before and (b) after the addition of K_3 [$Fe(CN)_6$] (2 mM); (B) photocurrent responses of BiOI/ITO electrode in solutions of (a) Tris-HCl, (b) PB NPs (50 μL) + Tris-HCl, (c) PB NPs (50 μL) + NaOH (100 μL) + Tris-HCl, and (d) PB@PDA NPs (50 μL) + NaOH (100 μL) + Tris-HCl; (C) proposed mechanism of electron transfer at the BiOI/ITO electrode. (D) UV–vis absorption spectra of (a) PB@PDA NPs (50 μL) + H_2O (100 μL) and (b) PB@PDA NPs (50 μL) + NaOH (100 μL), with the inset showing the change in color of the PB NP solution upon the addition of NaOH. [Tris-HCl solution, 0.01 M and pH = 7.4; PB NP and PB@PDA NP dispersions, 1 mg mL^{-1}; NaOH solution, 0.1 M]. (For interpretation of the references to color in this figure legend, the reader is referred to the Web version of this article.)

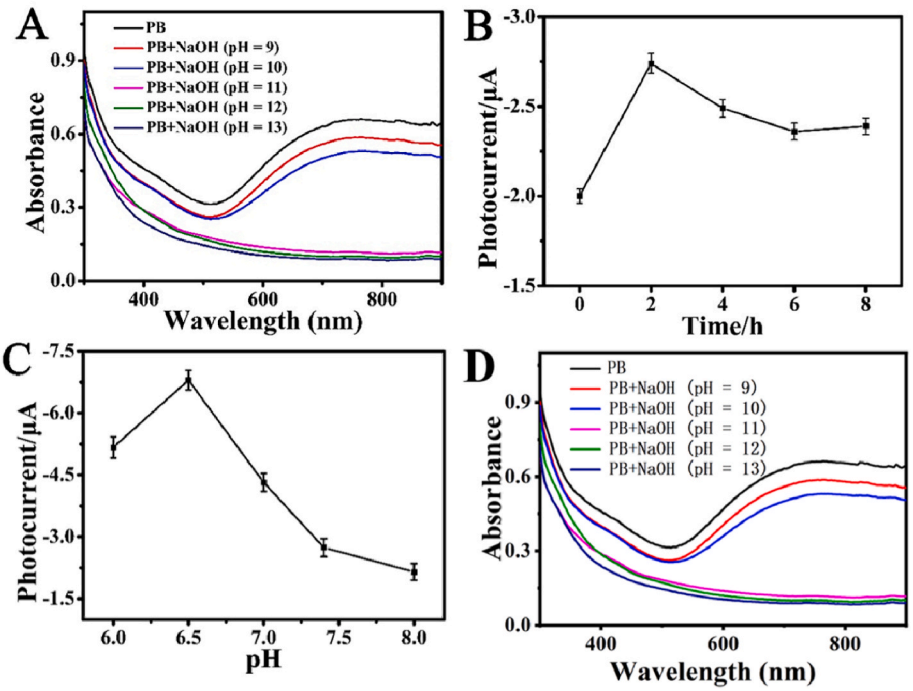

Fig. 4. (A) UV–vis absorption spectra of PB NP dispersions containing NaOH solutions with different pH values; (B) photocurrent response of PB NPs coated with PDA films for different durations; (C) photocurrent response of BiOI electrode in solutions of PB@PDA NPs + NaOH + Tris-HCl with different pH values; (D) UV–vis absorption spectra of PB@PDA NPs + NaOH in Tris-HCl solutions with different pH values; Hundred microliter PB NP dispersions were used for (A), whereas 1 mg/mL PB NP and PB@PDA NP dispersions (50 μL) were used for (B)–(D); the Tris-HCl concentration was 0.01 M (pH = 7.4), whereas that of NaOH was 0.1 M.

4. Conclusions

A novel sandwich-type cathodic photoelectrochemical immunosensor was designed using the p-type semiconductor BiOI as the photoelectrode and PB@PDA NPs as the secondary antibody marker for CEA detection. PDA film coating enabled the PB NPs to readily capture the CEA antibody, whereas both PDA and PB contribute to the enhancement of cathodic PEC responses and good analytical performances were achieved. The separated construction strategy also enables the sensor to have a lower detection limit. The constructed sensor showed good performance for the detection of CEA with a detection range of 0.001–100 ng mL^{-1} and a detection limit of 54.9 fg mL^{-1}, and showed excellent detection performance in actual sample detection. This strategy of controlling the release of electron donors/acceptors by relying on labels has broad application prospects for the design and preparation of PEC biosensors.

Credit author statement

Xiaodi Zhu: Investigation, Conceptualization, Methodology, Writing - original draft. **Jingkai Shan:** Data curation. **Li Dai:** Software. **Feifei Shi:** Software. **Jinshen Wang:** Project administration, Funding

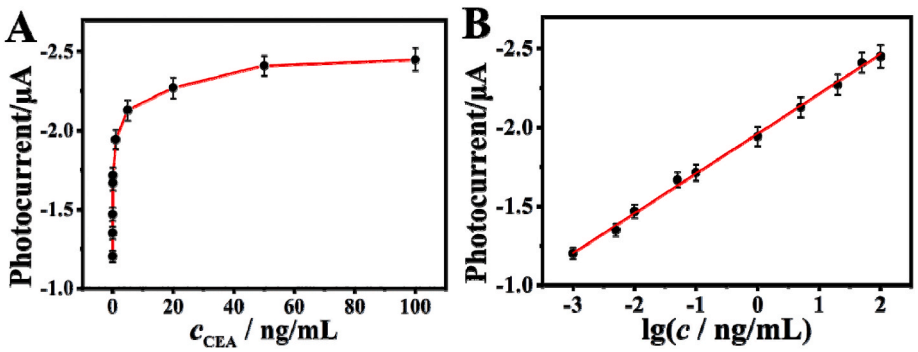

Fig. 5. (A) Photocurrent response of the constructed PEC sensor to different CEA concentrations (0.001, 0.005, 0.01, 0.05, 0.1, 1, 5, 20, 50, and 100 ng mL^{-1}); (B) linear relationship between photocurrent and the logarithm of CEA concentration.

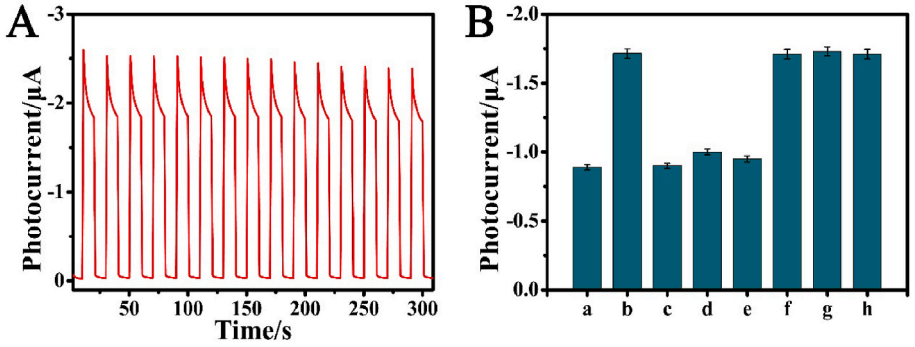

Fig. 6. (A) Photocurrent response of the PEC biosensor to 0.1 ng mL^{-1} CEA with 15 switching cycles at 10 s intervals; (B) anti-interference tests of the PEC biosensor with the following specimens: (a) blank, (b) 0.1 ng mL^{-1} CEA, (c) 10 ng mL^{-1} NSE, (d) 10 ng mL^{-1} CD44, (e) 10 ng mL^{-1} IgG, (f) 0.1 ng mL^{-1} CEA + 10 ng mL^{-1} NSE, (g) 0.1 ng mL^{-1} CEA + 10 ng mL^{-1} CD44, and (h) 0.1 ng mL^{-1} CEA + 10 ng mL^{-1} IgG.

Table 1
Comparison with previously reported CEA detection parameters.

Method	Linear range (ng·mL^{-1})	Detection limit (ng·mL^{-1})	Reference
Electrochemical	0.1–100000	0.8	[39]
Electrochemical	0.1–1000	0.6	[40]
Fluorescent	5.0–100	0.000085	[41]
Fluorescent	0.05–2	0.03	[42]
Colorimetry	0.2–2.5	0.03	[43]
Colorimetry	0.05–100	0.0211	[44]
Enzyme-linked (ELISA)	0.0313–8.0	0.0075	[45]
Photoelectrochemical	0.05–5	0.0112	[46]
Photoelectrochemical	0.005–20	0.0014	[47]
Photoelectrochemical	0.005–50	0.001	[48]
Photoelectrochemical	0.001–100	0.0000549	Present study

Table 2
Determination of CEA in the human serum sample.

Sample	content of CEA in the serum (ng·mL^{-1})	the addition content (ng·mL^{-1})	the average of the detected concentrations (ng·mL^{-1})	RSD (%, n = 5)	recovery (%, n = 5)
A	10	5.0	15	1.5	100.0
		10	20	2.3	100.0
		20	29	1.6	95.0
B	0.060	0.10	0.16	1.3	100.0
		0.20	0.27	1.1	105.0
		0.30	0.37	1.1	103.3

acquisition. **Huan Wang:** Resources. **Yuyang Li:** Resources. **Dan Wu:** Resources. **Hongmin Ma:** Writing - review & editing, Project administration, Funding acquisition. **Qin Wei:** Resources. **Huangxian Ju:** Funding acquisition.

Declaration of competing interest

The authors declare that they have no known competing financial interests or personal relationships that could have appeared to influence the work reported in this paper.

Data availability

No data was used for the research described in the article.

Acknowledgments

This work was financially supported by the Shandong Provincial Natural Science Foundation (ZR2020YQ13, ZR2020MH221), the National Natural Science Foundation of China (21890741), a Project of Shandong Province Higher Educational Youth Innovation Science and Technology Program (2020KJC008), the Jinan Scientific Research Leader Workshop Project (2020GXRC048), and the Young Taishan Scholars Program of Shandong Province of China.

References

[1] X. Pei, B. Zhang, J. Tang, B. Liu, W. Lai, D. Tang, Sandwich-type immunosensors and immunoassays exploiting nanostructure labels: a review, Anal. Chim. Acta 758 (2013) 1–18, https://doi.org/10.1016/j.aca.2012.10.060.
[2] H. Filik, A.A. Avan, Nanostructures for nonlabeled and labeled electrochemical immunosensors: simultaneous electrochemical detection of cancer markers: a

review, Talanta 205 (2019), 120153, https://doi.org/10.1016/j.talanta.2019.120153.
[3] S.D. Gan, K.R. Patel, Enzyme immunoassay and enzyme-linked immunosorbent assay, J. Invest. Dermatol. 133 (2013) 1–3, https://doi.org/10.1038/jid.2013.287.
[4] J. Wang, W. Lv, J. Wu, H. Li, F. Li, Electropolymerization-induced positively charged phenothiazine polymer photoelectrode for highly sensitive photoelectrochemical biosensing, Microchim. Acta 91 (2019) 13831–13837, https://doi.org/10.1021/acs.analchem.9b03311.
[5] L. Qu, X. Ren, D. Fan, X. Kuang, X. Sun, B. Wang, Q. Wei, H. Ju, Split-type electrochemical immunoassay system triggering ascorbic acid-mediated signal magnification based on a controlled-release strategy, ACS Appl. Mater. Interfaces 13 (2021) 29179–29186, https://doi.org/10.1021/acsami.1c07780.
[6] Y. Sun, P. Xiong, J. Tang, Z. Zeng, D. Tang, Ultrasensitive split-type electrochemical sensing platform for sensitive determination of organophosphorus pesticides based on MnO2 nanoflower-electron mediator as a signal transduction system, Anal. Bioanal. Chem. 412 (2020) 6939–6945, https://doi.org/10.1007/s00216-020-02824-0.
[7] Z. Huang, S. Yu, M. Jian, Z. Weng, H. Deng, H. Peng, W. Chen, Ultrasensitive glutathione-mediated facile split-type electrochemiluminescence nanoswitch sensing platform, Anal. Chem. 94 (2022) 2341–2347, https://doi.org/10.1021/acs.analchem.1c05198.
[8] J. Zhuang, D. Tang, W. Lai, M. Xu, D. Tang, Target-induced nano-enzyme reactor mediated hole-trapping for high-throughput immunoassay based on a split-type photoelectrochemical detection strategy, Anal. Chem. 87 (2015) 9473–9480, https://doi.org/10.1021/acs.analchem.5b02676.
[9] J.-T. Cao, X.-L. Fu, L.-Z. Zhao, S.-H. Ma, Y.-M. Liu, Highly efficient resonance energy transfer in g-C3N4-Ag nanostructure: proof-of-concept toward sensitive split-type electrochemiluminescence immunoassay, Sensor. Actuator. B Chem. 311 (2020), 127926, https://doi.org/10.1016/j.snb.2020.127926.
[10] G. Wang, F. Yuan, T. Gu, Y. Dong, Q. Wang, W. Zhao, Enzyme-initiated quinone-chitosan conjugation chemistry: toward a general in situ strategy for high-throughput photoelectrochemical enzymatic bioanalysis, Anal. Chem. 90 (2018) 1492–1497, https://doi.org/10.1021/acs.analchem.7b04625.
[11] K. Zhang, S. Lv, Z. Lin, M. Li, D. Tang, Bio-bar-code-based photoelectrochemical immunoassay for sensitive detection of prostate-specific antigen using rolling circle amplification and enzymatic biocatalytic precipitation, Biosens. Bioelectron. 101 (2018) 159–166, https://doi.org/10.1016/j.bios.2017.10.031.
[12] J. Zhuang, B. Han, W. Liu, J. Zhou, K. Liu, D. Yang, D. Tang, Liposome-amplified photoelectrochemical immunoassay for highly sensitive monitoring of disease biomarkers based on a split-type strategy, Biosens. Bioelectron. 99 (2018) 230–236, https://doi.org/10.1016/j.bios.2017.07.067.
[13] W. Zhao, J. Xu, H. Chen, Photoelectrochemical immunoassays, Anal. Chem. 90 (2018) 615–627, https://doi.org/10.1021/acs.analchem.7b04672.
[14] G. Yang, Z. Xiao, C. Tang, Y. Deng, H. Huang, Z. He, Recent advances in biosensor for detection of lung cancer biomarkers, Biosens, Bioelectron 141 (2019), 111416, https://doi.org/10.1016/j.bios.2019.111416.
[15] H. Li, J. Wang, X. Wang, H. Lin, F. Li, Perylene-based photoactive material as a double-stranded DNA intercalating probe for ultrasensitive photoelectrochemical biosensing, ACS Appl. Mater. Interfaces 11 (2019) 16958–16964, https://doi.org/10.1021/acsami.9b04299.
[16] H. Wang, F. Li, Y. Dong, Z. Li, G.-L. Wang, Ferricyanide stimulated cathodic photoelectrochemistry of flower-like bismuth oxyiodide under ambient air: a general strategy for robust bioanalysis, Sensor. Actuator. B Chem. 288 (2019) 683–690, https://doi.org/10.1016/j.snb.2019.03.066.
[17] H. Wang, F. Yuan, X. Wu, Y. Dong, G.L. Wang, Enzymatic in situ generation of covalently conjugated electron acceptor of PbSe quantum dots for high throughput and versatile photoelectrochemical bioanalysis, Anal. Chim. Acta 1058 (2019) 1–8, https://doi.org/10.1016/j.aca.2019.01.057.
[18] V.D. Ivanov, Four decades of electrochemical investigation of Prussian blue, Ionics 26 (2019) 531–547, https://doi.org/10.1007/s11581-019-03292-y.
[19] Y. Zhao, Q. Zhai, D. Dong, T. An, S. Gong, Q. Shi, W. Cheng, Highly stretchable and strain-insensitive fiber-based wearable electrochemical biosensor to monitor glucose in the sweat, Anal. Chem. 91 (2019) 6569–6576, https://doi.org/10.1021/acs.analchem.9b00152.
[20] F. Arduini, S. Cinti, V. Caratelli, L. Amendola, G. Palleschi, D. Moscone, Origami multiple paper-based electrochemical biosensors for pesticide detection, Biosens. Bioelectron. 126 (2019) 346–354, https://doi.org/10.1016/j.bios.2018.10.014.
[21] P. Ni, Y. Sun, H. Dai, W. Lu, S. Jiang, Y. Wang, et al., Prussian blue nanocubes peroxidase mimetic-based colorimetric assay for screening acetylcholinesterase activity and its inhibitor, Sensor. Actuator. B Chem. 240 (2017) 1314–1320, https://doi.org/10.1016/j.snb.2016.09.048.
[22] D. Lu, H. Jiang, G. Zhang, Q. Luo, Q. Zhao, X. Shi, An in situ generated prussian blue nanoparticle-mediated multimode nanozyme-linked immunosorbent assay for the detection of Aflatoxin B1, ACS Appl. Mater. Interfaces 13 (2021) 25738–25747, https://doi.org/10.1021/acsami.1c04751.
[23] S. Jansod, T. Cherubini, Y. Soda, E. Bakker, Optical sensing with a potentiometric sensing array by prussian blue film integrated closed bipolar electrodes, Anal. Chem. 92 (2020) 9138–9145, https://doi.org/10.1021/acs.analchem.0c01421.
[24] H. Lee, S.M. Dellatore, W.M. Miller, P.B. Messersmith, Mussel-inspired surface chemistry for multifunctional coatings, Science 318 (2007) 426–430, https://doi.org/10.1126/science.1147241.
[25] B. Fan, Q. Fan, M. Cui, T. Wu, J. Wang, H. Ma, Q. Wei, Photoelectrochemical biosensor for sensitive detection of soluble CD44 based on the facile construction of a poly(ethylene glycol)/hyaluronic acid hybrid antifouling interface, ACS Appl. Mater. Interfaces 11 (2019) 24764–24770, https://doi.org/10.1021/acsami.9b06937.
[26] B. Fan, Q. Fan, L. Hu, M. Cui, X. Wang, H. Ma, Q. Wei, Polydopamine-PEG-folic acid conjugate film engineered TiO2 nanotube Arrays for photoelectrochemical sensing of folate binding protein, ACS Appl. Mater. Interfaces 12 (2020) 1877–1884, https://doi.org/10.1021/acsami.9b17630.
[27] N. Gao, X. Wang, J. Feng, X. Li, H. Wang, D. Fan, Y. Zhang, H. Ma, Q. Wei, H. Ju, Sphere-on-tube biomimetic hierarchical nanostructures coupled with engineered surfaces for enhanced photoelectrochemical biosensing of cancer cells expressing folate receptors, Adv. Mater. Interfac. 8 (2021), 2100421, https://doi.org/10.1002/admi.202100421.
[28] M. Wang, B. Li, Y. Du, H. Bu, Y. Tang, Q. Huang, Fluorescence imaging-guided cancer photothermal therapy using polydopamine and graphene quantum dot-capped Prussian blue nanocubes, RSC Adv. 11 (2021) 8420–8429, https://doi.org/10.1039/D0RA10491D.
[29] Y. Wang, X. Pang, J. Wang, Y. Cheng, Y. Song, Q. Sun, Q. You, F. Tan, J. Li, N. Li, Magnetically-targeted and near infrared fluorescence/magnetic resonance/photoacoustic imaging-guided combinational anti-tumor phototherapy based on polydopamine-capped magnetic Prussian blue nanoparticles, J. Mater. Chem. 6 (2018) 2460–2473, https://doi.org/10.1039/C8TB00483H.
[30] C. Tong, X. Zhong, Y. Yang, X. Liu, G. Zhong, C. Xiao, B. Liu, W. Wang, X. Yang, PB@PDA@Ag nanosystem for synergistically eradicating MRSA and accelerating diabetic wound healing assisted with laser irradiation, Biomaterials 243 (2020), 119936, https://doi.org/10.1016/j.biomaterials.2020.119936.
[31] X. Lin, Y. Cao, J. Li, D. Zheng, S. Lan, Y. Xue, F. Yu, M. Wu, X. Zhu, Folic acid-modified Prussian blue/polydopamine nanoparticles as an MRI agent for use in targeted chemo/photothermal therapy, Biomater. Sci. 7 (2019) 2996–3006, https://doi.org/10.1039/C9BM00276F.
[32] M. Xu, H. Gao, Q. Ji, B. Chi, L. He, Q. Song, Z. Xu, L. Li, J. Wang, Construction multifunctional nanozyme for synergistic catalytic therapy and phototherapy based on controllable performance, J. Colloid Interface Sci. 609 (2022) 364–374, https://doi.org/10.1016/j.jcis.2021.11.183.
[33] Y. Yang, Q. Liu, Y. Liu, J. Cui, H. Liu, P. Wang, Y. Li, L. Chen, Z. Zhao, Y. Dong, A novel label-free electrochemical immunosensor based on functionalized nitrogen-doped graphene quantum dots for carcinoembryonic antigen detection, Biosens. Bioelectron. 90 (2017) 31–38, https://doi.org/10.1016/j.bios.2016.11.029.
[34] P. Thomas, A. Gangopadhyay, G. Steele, C. Andrews, H. Nakazato, S. Oikawa, J. Jessup, The effect of transfection of the CEA gene on the metastatic behavior of the human colorectal cancer cell line MIP-101, Cancer Lett. 92 (1995) 59–66, https://doi.org/10.1016/0304-3835(95)03764-N.
[35] S. Hammarstrom, The carcinoembryonic antigen CEA family: structures, suggested functions and expression in normal and malignant tissues, Semin, Cancer Biol 9 (1999) 67–81, https://doi.org/10.1006/scbi.1998.0119.
[36] J. Hu, S. Weng, Z. Zheng, Z. Pei, M. Huang, P. Liu, Solvents mediated-synthesis of BiOI photocatalysts with tunable morphologies and their visible-light driven photocatalytic performances in removing of arsenic from water, J. Hazard Mater. 264 (2014) 293–302, https://doi.org/10.1016/j.jhazmat.2013.11.027.
[37] B. Zhao, Q. Huang, L. Dou, T. Bu, K. Chen, Q. Yang, L. Yan, J. Wang, D. Zhang, Prussian blue nanoparticles based lateral flow assay for high sensitive determination of clenbuterol, Sensor. Actuator. B Chem. 275 (2018) 223–229, https://doi.org/10.1016/j.snb.2018.08.029.
[38] M.E. Lynge, R. van der Westen, A. Postma, B. Städler, Polydopamine—a nature-inspired polymer coating for biomedical science, Nanoscale 3 (2011) 4916–4928, https://doi.org/10.1039/C1NR10969C.
[39] L.P.T. Carneiro, N.S. Ferreira, A.P.M. Tavares, A. Pinto, A. Mendes, M.G.F. Sales, A passive direct methanol fuel cell as transducer of an electrochemical sensor, applied to the detection of carcinoembryonic antigen, Biosens. Bioelectron. 175 (2021), 112877, https://doi.org/10.1016/j.bios.2020.112877.
[40] Y. Li, Y. Chen, D. Deng, L. Luo, H. He, Z. Wang, Water-dispersible graphene/amphiphilic pyrene derivative nanocomposite: high AuNPs loading capacity for CEA electrochemical immunosensing, Sensor. Actuator. B Chem. 248 (2017) 966–972, https://doi.org/10.1016/j.snb.2017.02.138.
[41] M. Iwanaga, All-dielectric metasurface fluorescence biosensors for high-sensitivity antibody/antigen detection, ACS Nano 14 (2020) 17458–17467, https://doi.org/10.1021/acsnano.0c07722.
[42] M. Chen, C. Ma, H. Zhao, Y. Yan, Exonuclease III-assisted fluorometric aptasensor for the carcinoembryonic antigen using graphene oxide and 2-aminopurine, Microchim, Acta 186 (2019) 500, https://doi.org/10.1007/s00604-019-3621-4.
[43] X. Wang, B. Zhang, J. Li, H. Chang, W. Wei, A simple and fast chromogenic reaction based on Ag3PO4/Ag nanocomposite for tumor marker detection, Talanta 175 (2017) 229–234, https://doi.org/10.1016/j.talanta.2017.07.039.
[44] P. Wang, Y. Tang, X. Wen, R. Amal, Y.H. Ng, Enhanced visible light-induced charge separation and charge transport in Cu_2O-based photocathodes by urea treatment, ACS Appl. Mater. Interfaces 7 (2015) 19887–19893, https://doi.org/10.1021/acsami.5b06601.
[45] Z. He, J. Huffman, K. Curtin, K.L. Garner, E.C. Bowdridge, X. Li, T.R. Nurkiewicz, P. Li, Composable microfluidic plates (cplate): a simple and scalable fluid manipulation system for multiplexed enzyme-linked immunosorbent assay (ELISA), Anal. Chem. 93 (2021) 1489–1497, https://doi.org/10.1021/acs.analchem.0c03651.
[46] C. Wang, Y. Wang, H. Zhang, H. Deng, X. Xiong, C. Li, W. Li, Molecularly imprinted photoelectrochemical sensor for carcinoembryonic antigen based on polymerized

ionic liquid hydrogel and hollow gold nanoballs/$MoSe_2$ nanosheets, Anal. Chim. Acta 1090 (2019) 64–71, https://doi.org/10.1016/j.aca.2019.09.029.

[47] S. Wu, H. Tan, C. Wang, J. Wang, S. Sheng, A colorimetric immunoassay based on coordination polymer composite for the detection of carcinoembryonic antigen, ACS Appl. Mater. Interfaces 11 (2019) 43031–43038, https://doi.org/10.1021/acsami.9b18472.

[48] Y. Chen, M. Zhou, J. Yang, Y. Tan, W. Deng, Q. Xie, Tailoring the photoelectrochemical activity of hexametaphosphate-capped CdS quantum dots by Ca(2+)-triggered surface charge regulation: a new signaling strategy for sensitive immunoassay, Anal. Chem. 93 (2021) 13783–13790, https://doi.org/10.1021/acs.analchem.1c02284.